HYDRAULIC ACTUATOR SYSTEM FOR ROTOR CONTROL

Heinz Ulbrich* and Josef Althaus
Institute B of Mechanics
Technical University of Munich
P.O. Box 202420
D-8000 Munich 2, Federal Republic of Germany

In the last ten years several different types of actuators have been developed and fabricated for active control of rotors. This paper deals with a special hydraulic actuator system capable of generating high forces to rotating shafts via conventional bearings. The actively controlled hydraulic force actuator features an electrohydraulic servo valve which can produce amplitudes and forces at high frequencies necessary for influencing rotor vibrations. The mathematical description will be given in detail. The experimental results attained verify the theoretical model. Simulations already indicate the usefulness of this compact device for application to a real rotor system.

1 Introduction

Rotating machinery can be found in many fields of the industrial world; many could be improved with regard to speed of rotors/shafts, weight, noise, longevity and last but not least, safety, by applying active vibration control. The key to success for active measures in the improvement of the dynamics of rotating machinery lies in the availability of suitable actuators which have to satisfy the following requirements: the actuator must be capable of amplitudes in the range of the vibration amplitudes to be influenced on the one hand, and possess an appropriate frequency characteristic on the other hand. In the literature many papers deal with magnetic actuators, e.g. [3,4,5]. Magnetic actuators require a relatively large amount of space compared to the attainable forces. This deficiency may be avoided by the use of hydraulically controlled chambers.

The main topic of this paper is the introduction of a newly developed hydraulic actuator which is able to apply forces to rotating shafts via the bearings. For producing forces (pressure variations) servo valves are used. The regulating distance is caused by elastic deformations of membranes (no cylinder piston arrangements).

All influences which could be of practical relevance (oil compressibility, dynamic effects of the servo valve and the fluid itself) are taken into account in the mathematical description of the system. Applying the theory of plates, the strain in the membranes can be calculated. A limitation of the actuator system is given by the permitted strain which may not be exceeded in any area. Because of the actuator dynamics an appropriate enlargement of the equations of motion for the entire system is necessary. The equations of the actuator dynamics show that the chamber system already applies damping effects to the rotor system without any control input. With the aid of a well adapted controller the damping of the entire system can be essentially improved. This is

*Presently at Technical University of Braunschweig, Braunschweig, Federal Republic of Germany.

demonstrated by simulations. The input parameters, especially with regard to the actuator system, have been determined by experiment.

For verifying the results achieved by computer simulations two different experimental test facilities have been constructed (see Fig. 4 and Fig. 5). One test rig contains the active chamber system. It allows the evaluation of its characteristic frequency. The experimental results which are attained verify the theoretical model. The second test facility consists of an elastic rotor structure and two different types of magnetic actuators. In further investigations the two test facilities will be combined in order to test the dynamic behavior of the elastic rotor controlled by the active chamber system.

Nomenclature

$\boldsymbol{A}$	system matrix
A^*	membrane area
b	coefficient of the actuator input
$\boldsymbol{B}$	control matrix
c, d	bearing coefficients
C_K	lag coefficient of the control force
c_L	membrane stiffness
d_L	passive damping coefficient of the actuator
$\boldsymbol{E}$	identity matrix
$\boldsymbol{h}$	force vector
K_{pq}	leakage coefficient
K_v	loop gain of the servo valve
K^*	constant of the oil compressibility and the membrane buckling
$\boldsymbol{M}, \boldsymbol{P}, \boldsymbol{Q}$	system matrices of the second order system
F^*	control force to the bearing housing
$\mathcal{F}_L$	transfer function describing the fluid dynamics and the stiffness
$\mathcal{F}_P$	transfer function of the chamber pressure
$\mathcal{F}_V$	transfer function considering the servo valve dynamics, the oil compressibility, and the membrane buckling
$\mathcal{F}_{valve}$	transfer function describing the servo valve dynamics
$\mathcal{F}_x$	transfer function of the regulating distance
$\boldsymbol{J}_L$	Jacobian matrix of translation of the bearing
ΔP	pressure drop in the valve
ΔP_S	supply pressure difference
ΔP_V	chamber pressure difference
$\boldsymbol{q}$	vector of generalized coordinates
Q	oil flow through the loaded servo valve
Q_V	oil flow through the unloaded servo valve
s	Laplace-operator
t	time
$\boldsymbol{u}$	control vector

U_V	control voltage to the servo valve
U_N	nominal voltage of the servo valve
z	state vector
x, y	acting directions
x_L, y_L	regulating distance (bearing deflection)
ω_V	natural frequency of the servo valve
Ω	rotor frequency
ξ_V	servo valve damping coefficient

2 Description of the Actuator Device

The device of this compact system is shown in Fig. 1 by a schematic. It consists of two components: a commercially-available servo valve, which is able to transform electrical signals into flow- and pressure variations of the hydraulic fluid, and an elastic chamber system, which transduces the pressure variations into displacements and into forces acting on the outer bearing housing (in Fig. 1 only one control direction is displayed).

The servo valve is supplied by the system pressure $\mathbf{P}$, which is to be kept constant, and the return pressure $\mathbf{R} \approx 0$. If the spool of the valve is in the neutral position (Fig. 1) the pressure in the chambers is half of the system pressure. After a shift of the spool by an input voltage $U_V \neq 0$, a pressure difference appears between the two output orifices. Because of the elasticity of the membranes this enables a shifting of the rotor in the radial direction. The chamber system itself consists of four cylindrical chambers which are equally spaced in a circle around the bearing housing. Each chamber is sealed on the top and bottom by an elastic membrane. In order to decouple forces into both acting directions, the bearing housing is supported against the membrane system by linear roller guides. The influence of friction is thereby reduced as well. Alternative support solutions are given by design variations. To eliminate the linear roller guides the bearing can be mounted via elastic rods to the outer housing. The two opposing chambers are both controlled by one servo valve (one valve per force direction).

This compact actuator system is capable of generating very large forces and can thereby influence even large turbines weighing several tons. Actuator pistons as an alternative to the deformable chambers have the drawback that they possess relatively large moving masses. In addition, sealing problems and friction forces on the contact surfaces would occur. All these influences have negative impacts on the frequency characteristic. An appropriate design of the membranes enables the desired amplitudes of motion without exceeding the stress limits of the material.

3 Theory

With the aid of the theory of plates the calculation of the stress in the membranes caused by a given load can be performed, e.g. [8]. Experiments have shown that the real stresses are always lower than the calculated stresses. This is caused by the elastic fixing of the membrane in the real

system compared to the theoretically stiff fixing. For calculating the stresses the load must be known. Therefore it is necessary to describe the dynamics of this active machine element.

3.1 Chamber System Dynamics

3.1.1 Servo Valve

The dynamics of the servo valves are given by the manufacturer (MOOG, see [2]) as a PT_2-element. The valve flow Q_V for the unloaded valve can be given as a function of the input voltage U_V in the *Laplace-domain* (with s as a complex variable)

$$Q_V = K_v \mathcal{F}_{valve} \cdot U_V \quad , \quad \mathcal{F}_{valve} = \frac{1}{1 + \frac{2\xi_v}{\omega_v} s + \frac{1}{\omega_v^2} s^2} \tag{1}$$

where K_v is the loop gain of the valve, which depends on the supply pressure $\Delta P_S = \boldsymbol{P} - \boldsymbol{R}$ (see Fig. 1) and the geometry of the valve itself, ω_v is the natural frequency of the valve, and ξ_v is the damping ratio of the valve. In the case where the valve is loaded, the fluid flow depends on the output pressure ΔP_V (load differential pressure). For this reason the equation for the fluid flow passing a pressure-regulating valve (here between the spool of the valve, inlet- and outlet orifice, see Fig. 1) is applied. In general the fluid flow Q is proportional to the square root of the differential pressure ΔP [1],

$$Q \sim \sqrt{\Delta P} \quad . \tag{2}$$

Applying the relation that the sum of the pressure drops in the valve ΔP and the load pressure ΔP_V is equal to the drop of the supply pressure ΔP_S,

$$\Delta P + \Delta P_V = \Delta P_S \quad , \tag{3}$$

and considering eq. 2 and the fluid flow properties in the valve we obtain

$$Q = Q_V \cdot \sqrt{1 - \frac{\Delta P_V}{\Delta P_S}} \quad . \tag{4}$$

After a linearization in the neighborhood of $\Delta P_V = 0$,eq. 4 becomes

$$Q = Q_V \; - \; K_{pq} \cdot \Delta P_V \quad , \quad K_{pq} \text{ leakage coefficient} \quad . \tag{5}$$

The linearization applied in eq. 5 is valid for $\Delta P_V \leq \frac{1}{2} \Delta P_S$ where K_{pq} is theoretically a function of Q_V. For low input voltage $U_V \leq \frac{1}{10} U_N$ (U_N = nominal voltage) this dependance can be neglected. Fig. 2 shows the course of the fluid flow Q as a function of Q_V and the differential pressure of the valve ΔP_V as given by the manufacturer. The slope of these curves at the operating point ($\Delta P_V = 0$) is given by K_{pq} appearing in eq. 5. In contrast to the nonlinear eq. 4 in practice one can establish that even at $U_V = 0$ (which results in $Q_V = 0$, eq. 1) the fluid flow is non-zero for $\Delta P_V \neq 0$. This is caused by leakage where the spool is in the neutral position. The linear eq. 5 takes this into account. Fig. 2 shows this behavior of the valve by the line through the origin with a slope which is non-zero. For derivation of the equation of motion and the transfer characteristic of the entire system (see later), the linear relation by eq. 5 is used. The nonlinearity of the relation between the fluid flow Q and the pressure drop ΔP_V can be taken into account by K_{pq} as a function of Q_V.

3.1.2 Influence of Fluid Flow, Membrane Stiffness and Oil Compressibility

The application of the continuity equation results in an additional relation for the fluid flow Q,

$$Q = A^* \cdot \dot{x}_L + K^* \cdot \Delta \dot{P}_V \quad . \tag{6}$$

A^* is the characteristic membrane area, and K^* represents the oil compressibility and the deformation of the membrane into a direction that doesn't lead to a movement of the bearing (membrane buckling), see Fig. 3. K^* is dependent on the oil volume V_L, the bulk modulus of the fluid β_K, and the membrane geometry characterized by K_M,

$$K^* = \frac{V_L}{4\beta_K} + K_M \quad . \tag{7}$$

Simulations have shown that the fluid losses caused by oil inertia, friction and losses at the inlet and outlet orifices are negligible. So the pressure difference at the outlet orifices of the valve is approximately equal to the chamber pressure difference, constant ΔP_V.

3.1.3 Recapitulation of Equations

The equilibrium of forces applied with respect to the membranes (entire arrangement of two membranes acting in one direction) leads to

$$F^* = A^* \cdot \Delta P_V - c_L \cdot x_L \quad , \tag{8}$$

where c_L is the entire membrane stiffness in the force direction and F^* the control force to the bearing housing, see Fig. 3. Including this equation we obtain F^* as a function of the control voltage U_V and the membrane deflection, respectively; the bearing displacement x_L in the direction of the force

$$F^* = \mathcal{F}_V \cdot U_V - \mathcal{F}_L \cdot x_L \quad . \tag{9}$$

$\mathcal{F}_V$ is the transfer function describing the dependence on the control voltage

$$\mathcal{F}_V = \mathcal{F}_{valve} \cdot \frac{\frac{A^* K_v}{K_{pq}}}{1 + C_K \cdot s} \quad , \tag{10}$$

and $\mathcal{F}_L$ is the transfer function considering the influences of the fluid dynamics and the stiffness of the arrangement

$$\mathcal{F}_L = \frac{\frac{A^{*2}}{K_{pq}} s}{1 + C_K \cdot s} + c_L \quad . \tag{11}$$

The constant C_K is represented by the leakage coefficient K_{pq} and by the oil compressibility and membrane buckling K^* eq. 7,

$$C_K = \frac{K^*}{K_{pq}} \quad . \tag{12}$$

3.1.4 Representation in Time Domain

For including the actuator system into the complete system, the representation of eq. 9 in the time-domain is more convenient. With the equations above we get a set of differential equations which describe the control force F^* as a function of the input voltage U_V and bearing displacement x_L,

$$\begin{aligned} F^* &= A^*\Delta P_V - c_L x_L \quad , \\ K^*\Delta\dot{P}_V + K_{pq}\Delta P_V + A^*\dot{x}_L &= Q_V \\ \frac{1}{\omega_v^2}\ddot{Q}_V + \frac{2\xi_v}{\omega_v}\dot{Q}_V + Q_V &= K_v U_V \quad . \end{aligned} \tag{13}$$

The coefficient c_L describes the additional stiffness effects with regard to the entire system (see later).

3.1.5 Simplification and Interpretation of Equations

For designing control concepts and to explain the fundamental operation, the equations will be simplified. In order to obtain a simple relationship between the control voltage U_V, the regulating distance x_L, and the control force F^*, the PT_2-behavior of the servo valve will be approximated by a linear relationship ($\mathcal{F}_{valve} = 1$). This is valid at frequencies under the cut–off frequency of the valve. This simplification leads to the following form

$$C_K\dot{F}^* + F^* = b \cdot U_V \; - \; c_L \cdot x_L \; - \; d_L \cdot \dot{x}_L \tag{14}$$

where $b = \frac{A^*K_v}{K_{pq}}$ and $d_L = \frac{A^{*2}}{K_{pq}} + C_K c_L$.

The constant C_K representing the oil compressibility and the membrane buckling in the equation above has an important influence. If C_K is negligible the actuator works as a passive spring and damper unit characterized by the coefficients c_L and d_L. Additionally a control force F_C acts that is proportional to the input voltage U_V (see Fig. 9). In the other case, if the frequency $\omega_K = \frac{1}{C_K}$ is below the frequency range of application, the actuator possesses an integral behavior. As a result the feedback of velocities and accelerations leads to stiffness and damping effects. In this case or if ω_K is inside the range of application (PT_1 behavior), a proportional behavior (see Fig. 9) can be achieved by an internal phase shifting controller (e.g. feedback of pressure ΔP_V) or an additional passive throttle between the two output orifices.

By an appropriate design of the membrane (constants c_L, A^*, K_M), of the oil volume V_L, of the supply pressure ΔP_S, and by the choice of the suitable valve size (constant K_v and K_{pq}), the actuator can be tuned in an optimal way. In the case of a sudden pressure drop ($\Delta P_S \rightarrow 0$) the rotor bearing is always sufficiently supported by an adequate membrane stiffness c_L.

3.1.6 Transfer Characteristic of Actuator

In the following the transfer characteristic of the complete actuator system is investigated applying a sinusoidal input voltage U_V to the valve. The purpose of this is to get a comparison to

the experiments which are described in chapter 3.1.6 and 5. The resulting outputs are the regulating distance x_L and the pressure difference ΔP_V between the opposing chambers. Introducing a mass which simulates the mass of the rotor, including the support system, the control force appearing in eq. 9 has to be equal to

$$F^* = m \; x_L \cdot s^2 \quad . \tag{15}$$

The transfer functions for the regulating distance $\mathcal{F}_x$ and the chamber pressure $\mathcal{F}_P$ can be expressed

$$\mathcal{F}_x = \frac{x_L}{U_V} = \frac{b \cdot \mathcal{F}_{valve}}{C_K m \cdot s^3 + m \cdot s^2 + d_L \cdot s + c_L} \quad , \tag{16}$$

$$\mathcal{F}_P = \frac{\Delta P_V}{U_V} = \frac{m \cdot s^2 + c_L}{A^*} \cdot \mathcal{F}_x \quad . \tag{17}$$

The coefficients b and d_L are given in eq. 14.

4 Test Facilities

Fig. 4 shows the test rig which was designed to investigate the chamber system experimentally. The investigation is conducted only in the vertical direction. The facility mainly consists of the housing 1 where the four oil chambers 2 are integrated. The distance rod 3 performs the function of the bearing housing and assures that the opposing chambers both move the same absolute distance. For investigating the influence of masses additional masses can be mounted on the distance rod 3. The influence of friction caused by the linear roller guides (see Fig. 1) can be studied by loading the chambers for the horizontal direction with an appropriate pressure in order to press the linear roller guides via distance sleeves 4 on the distance rod. The entire arrangement is mounted on the foundation including the servo valve 5. Servo valve and chambers are connected via pipes 6. Between actuator and hydraulic control unit (not shown in Fig. 4) are the connections to the first stage pressure unit, main control pressure unit (pressure **P** shown in Fig. 1), return pressure unit (indicated by pressure **R** in Fig. 1), and an additional pressure supply for the linear guiding bearings.

To enable a broad range of experimental investigations, variations of the supply pressure ΔP_S, membrane thickness h, contact pressure for the guiding bearings, additional masses m (see eq. 15) and of course the control voltage U_V (function generator) can be conducted.

The measurement equipment installed allows one to gather the following information: regulating distance with the aid of an inductive displacement sensor 7, and oil pressure in the chambers by piezo electric pressure sensors 8. Additional information is given by acceleration pick ups (not shown) mounted on the distance rod and by strain gauges to determine the strain of the membranes.

A special hydraulic unit was designed to assure that the supply pressure is constant. This is required because the fluid flow changes with frequencies up to 200 *Hz* and higher. These requirements can be met with the aid of a controllable radial piston pump and an appropriate reservoir.

The test rig shown in Fig. 5 is used to investigate different control concepts. It consists of an elastic rotor structure 9, a magnetic bearing 10 for simulating different excitation forces, the bearing unit 11, and actuator system which is presently realized by electromagnetic actuators 12. A further description of the test rig and the test results attained by this facility are given e.g. in [3].

The active chamber system will be integrated in the test facility Fig. 5 after conclusion of the experiments with the test rig Fig. 4. For this purpose the chambers for the horizontal direction have to be activated by a second servo valve, and the distance rod has to be replaced by the bearing unit. Finally the electromagnetic actuators 12 are substituted by the active chamber system.

5 Transfer Characteristic

In the following the transfer functions $\mathcal{F}_x$ and $\mathcal{F}_P$, eq. 16 and 17, for the regulating distance x_L and the chamber pressure ΔP_V will be investigated. The goal is to compare theoretical and experimental behavior of the actuator and to determine the system parameters. These are the membrane stiffness c_L, the leakage coefficient K_{pq}, the loop gain of the servo valve K_v and the coefficient K^* which describes the oil compressibility and the membrane buckling. The simulation is based on the data shown in Fig. 6 which are equivalent to the data of the test facility. The results can be seen in Fig. 7.

5.1 Theoretical Results

In the plot of the amplitude of the regulating distance in Fig. 7, one can recognize a PT_1 behavior up to a frequency of about 170 *Hz*. Its cut–off frequency is very low (about 2.2 *Hz*) and is given by $\frac{c_L}{d_L}$, see eq. 14. Beyond this frequency an extremum occurs in the amplitude at approximately 300 *Hz*. It corresponds to a pole in the transfer function of x_L and ΔP_V. This extremum results from a function $\alpha(s)$ which can be obtained by the denominator of eq. 16. This function has the value $\alpha(s) = 0$ at the frequency of $\omega_\alpha = 2\pi \cdot 287\ Hz$ $(s = i\omega)$,

$$\alpha(s) = m \cdot s^2 + \frac{m}{C_K} \cdot s + \frac{d_L}{C_K} = 0 \tag{18}$$

$$\Longrightarrow \quad \omega_\alpha = \sqrt{\frac{d_L}{C_K m} - \frac{1}{4C_K^2}} \approx \sqrt{\frac{A^{*2}}{K^* m}} \quad . \tag{19}$$

Eq. 19 shows that this frequency is mainly dependent on the membrane area A^*, on the mass m (simulating the rotor mass including the bearing unit) and on the oil compressibility and membrane buckling K^*. The servo valve has no influence. The expression $\frac{A^{*2}}{K^*}$ can be interpreted as a spring coefficient of the oil support and the membrane buckling. This natural frequency causes a phase shift of 180°. The rest of the curve is characterized by a drop in the amplitude due to the PT_2-behavior of the servo valve, see chapter 3.1.5. In the plot of the chamber pressure a further zero point can be seen at 110 *Hz*. It corresponds to the natural frequency of the one-DOF-oscillator, function $\beta(s)$ from eq. 17

$$\beta(s) = m \cdot s^2 + c_L = 0 \tag{20}$$

$$\Longrightarrow \quad \omega_\beta = \sqrt{\frac{c_L}{m}} \quad . \tag{21}$$

This characteristic frequency has no effect on the regulating distance and on the controllability of the rotor system.

5.2 Comparison of Theory and Experiment

Fig. 8 shows the measurements of the regulating distance x_L and chamber pressure ΔP_V. The results are obtained by noise excitation for the input voltage U_V.

A comparison with the results attained by theory shows good agreement. The characteristic frequencies at 110 *Hz* and 293 *Hz* are due to the effects described above (functions $\alpha(s)$ and $\beta(s)$, eq. 19 and 21). This shows that all important influences on the transfer characteristic are included in the transfer functions eq. 16 and 17. The step shaped curve at lower frequencies is only caused by the discrete evaluation of the output signals by the measurement electronics.

Measurements of the transfer characteristic of the servo valve (described by a PT_2-system) showed a better amplitude behavior at frequencies beyond the cut–off frequency than predicted by the PT_2-behavior.

The experiments have shown that the simplified equations for describing the performance of the active chamber system, eq. 14, are valid up to the cut–off frequency of the servo valve (here about 200 *Hz*), see chapter 3.1.5. For a higher frequency range it is necessary to use a servo valve with a higher cut–off frequency and to minimize the oil compressibility and the membrane buckling by minimizing the oil volume and by an appropriate design of the membrane.

6 Example of Application of the Actuator

6.1 Formulation of the Complete System

In designing a controller, a complete mathematical formulation of the system is assumed. A very efficient method of describing the rotor system to be controlled is modeling it as a hybrid multibody system (see [6]). This leads to the second order differential equation

$$\boldsymbol{M}\ddot{\boldsymbol{q}}(t) + \boldsymbol{P}\dot{\boldsymbol{q}}(t) + \boldsymbol{Q}\boldsymbol{q}(t) = \sum_i \boldsymbol{h}_i(\boldsymbol{q}, \dot{\boldsymbol{q}}, \ddot{\boldsymbol{q}}, \Omega, t) \tag{22}$$

with the vector $\boldsymbol{q} \in \mathbb{R}^f$ of the generalized minimal coordinates (f is the number of degrees of freedom), $\boldsymbol{M} \in \mathbb{R}^{f,f}$ is the mass matrix, $\boldsymbol{P} \in \mathbb{R}^{f,f}$ is the matrix of velocity–proportional forces, $\boldsymbol{Q} \in \mathbb{R}^{f,f}$ is the matrix taking into account the displacement–proportional forces, $\boldsymbol{h}_i \in \mathbb{R}^f$ is the vector of the i-th external force (e.g. control force), Ω is the rotor frequency and t indicates the time.

The control forces acting indirectly (via the rigid bearing unit) on the rotor can be expressed by

$$\boldsymbol{h}_B = \boldsymbol{J}_L^T \cdot \begin{bmatrix} F_x^* \\ F_y^* \end{bmatrix} \quad , \tag{23}$$

where $\boldsymbol{J}_L \in \mathbb{R}^{2,f}$ is the Jacobian matrix of translation belonging to the subsystem bearing unit and F_x^* and F_y^* the control forces given by differential eq. 13 acting in the x- and y-directions. The radial movement of the bearing described by x_L and y_L (perpendicular to x_L) can be formulated with the

aid of the Jacobian-matrix as

$$\begin{bmatrix} x_L \\ y_L \end{bmatrix} = \boldsymbol{J}_L \cdot \boldsymbol{q} \quad . \tag{24}$$

Introducing an enlarged state space vector

$$\boldsymbol{z} = \left[\boldsymbol{q}^T, Q_{Vx}, Q_{Vy}, \dot{\boldsymbol{q}}^T, \dot{Q}_{Vx}, \dot{Q}_{Vy}, \Delta P_{Vx}, \Delta P_{Vy}\right]^T \quad , \quad \boldsymbol{z} \in \mathbb{R}^{2f+6} \quad , \tag{25}$$

with Q_{Vx}, Q_{Vy} as the valve flow serving the x- and y-directions, respectively (eq. 1), and ΔP_{Vx}, ΔP_{Vy} as the valve output pressure supplying the x- and y-directions, respectively, we obtain the state equation

$$\dot{\boldsymbol{z}} = \boldsymbol{A}\boldsymbol{z} + \boldsymbol{B}\boldsymbol{u} \quad , \tag{26}$$

where $\boldsymbol{A}$ represents the system matrix, $\boldsymbol{B}$ the control matrix and

$$\boldsymbol{u} = [U_{Vx}, U_{Vy}]^T \tag{27}$$

the control vector consisting of the control voltages U_{Vx} proper for x- and U_{Vy} proper for the y-direction.

The matrices used in eq. 26 can be expressed as follows

$$\boldsymbol{A} = \begin{bmatrix} 0 & 0 & \boldsymbol{E}_f & 0 & 0 \\ 0 & 0 & 0 & \boldsymbol{E}_2 & 0 \\ -\boldsymbol{M}^{-1}\overline{\boldsymbol{Q}} & 0 & -\boldsymbol{M}^{-1}\boldsymbol{P} & 0 & \boldsymbol{M}^{-1}\boldsymbol{J}_L^T A^* \\ 0 & -\omega_v^2 \boldsymbol{E}_2 & 0 & -2\xi_v\omega_v \boldsymbol{E}_2 & 0 \\ 0 & \frac{1}{K^*}\boldsymbol{E}_2 & -\frac{A^*}{K^*}\boldsymbol{J}_L & 0 & -\frac{K_{pq}}{K^*}\boldsymbol{E}_2 \end{bmatrix} \quad , \tag{28}$$

$$\boldsymbol{B} = \begin{bmatrix} 0 \\ 0 \\ 0 \\ K_v\omega_v^2 \boldsymbol{E}_2 \\ 0 \end{bmatrix} \quad , \tag{29}$$

where the submatrix $\overline{\boldsymbol{Q}}$ is

$$\overline{\boldsymbol{Q}} = \boldsymbol{Q} + \boldsymbol{J}_L^T \boldsymbol{J}_L \cdot c_L \quad . \tag{30}$$

c_L is the membrane stiffness appearing in eq. 13 and $\boldsymbol{M}$, $\boldsymbol{P}$, $\boldsymbol{Q}$ are the system matrices from eq. 22. The matrix $\boldsymbol{E}_j \in \mathbb{R}^{j,j}$ represents the identity matrix.

6.2 Amplitude Characteristic of the Rotor

A simple rotor running in journal bearings is used. The rotor is supported by the active chamber system on its left side (Fig. 9). In the modeling of the rotor system, mass-, stiffness-, and gyroscopic effects and additional damping by the journal bearings are considered. As admissible shape functions only two mode shapes are taken into account. In most cases higher modes of real rotor systems are damped very well because of bearings or material damping.

In Fig. 10 are plotted frequency response functions versus rotor frequency. The exciting force is caused by an unbalance of the rotor. In Fig. 10a the scaled amplitudes $\frac{A}{A_o}$ at the runner position are displayed without active forces (solid line) and with active forces (dotted line). Fig. 10b shows the scaled nutation angles $\frac{\varphi}{\varphi_o}$ (slope of the elastic line) at the same location. The displacement amplitude shows a significant peak at the first natural frequency (bending vibration) and at the second natural frequency (nutation, indicated by the nutation angle). The feedback is realized by displacement, velocity, and pressure signals taken only at the actuator location. The controller was designed as a "constant controller" for the rotor frequency 100 *Hz*. Using this very simple controller, the results already demonstrate that a considerable reduction of the resonance amplitudes can be achieved.

7 Conclusion Remarks

The key to attaining the desired influence on the dynamics of rotor systems lies in the availability of suitable actuators. The development of the active chamber systems introduced in this paper will be an essential step towards industrial applications. This actuator works as a spring (membrane stiffness) and damper (hydraulic effects in the servo valve), and in addition to these passive forces a control force is acting proportional to the input voltage at the servo valve. One of the main goals of the paper is to confirm the theoretical model of this new actuator concept by experiment. The theoretical and experimental results achieved by these investigations show a very good conformity. Further experimental investigations of the actuator system included in the rotor system will demonstrate the usefulness of applying this active machine element for active vibration control of rotors. The use of a more sophisticated controller (additional measurement information, adaptive controller realized by special electronic equipment, hybrid controller) will show a wide range of possible applications for such an actuator device.

References

[1] ANDERSON, W.R.: Controlling Electrohydraulic Systems. Marcel Dekker, Inc. New York and Basel, 1988.

[2] THAYER, W.J.: Transfer Functions for Moog Servo Valves. Technical bulletin 103, Moog Inc. Controls Devision, East Aurora, N.Y. 14052, 1965.

[3] FÜRST, S.; ULBRICH, H.: An Active Support System for Rotors with Oil- Film Bearing. 4th International Conference on Vibration in Rotation Machinery of the Institution of Mechanical Engineers, Edinburgh, Scotland. Paper C 261/88, 1988, pp. 61–68.

[4] INNERHOFER, G; HAMMER, J.: Low-Cost Magnetic Bearing Reaction Wheel. Proc. of the IFAC Symp., Oxford, England, 1980.

[5] LIARD,G.: Aktive Magnetlager – ein Schlüssel zu höheren Spindeldrehzahlen. Kugellager-Zeitschrift 56, 213, 1982, pp. 8 - 13.

[6] ULBRICH, H.: Dynamik und Regelung von Rotorsystemen. Fortschr.-Ber. VDI-Z, Reihe 11, NR. 86, 1986.

[7] ULBRICH, H; ALTHAUS, J.: Actuator Design for Rotor Control. Twelfth biennial ASME Conference on Mechanical Vibration and Noise , Montreal, Canada, Sept. 17-20, 1989.

[8] TIMOSHENKO, S.; WOINOWSKY-KRIEGER, S.: Theorie of Plates and Shells. New York, Toronto, London, McGraw-Hill Book Company, 1959.

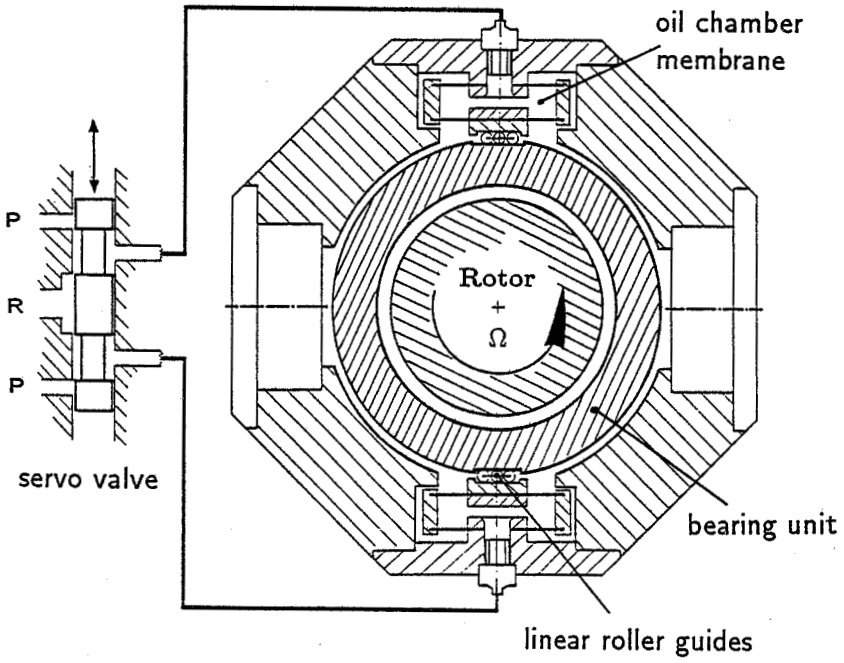

Figure 1: Active chamber system with servo valve

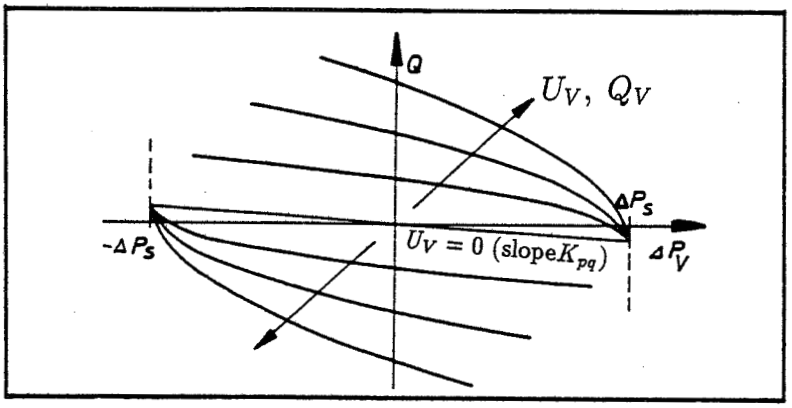

Figure 2: Fluid flow through the valve under load

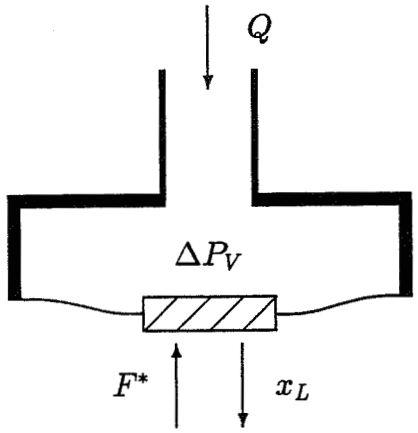

Figure 3: Model of the chamber and elastic membrane

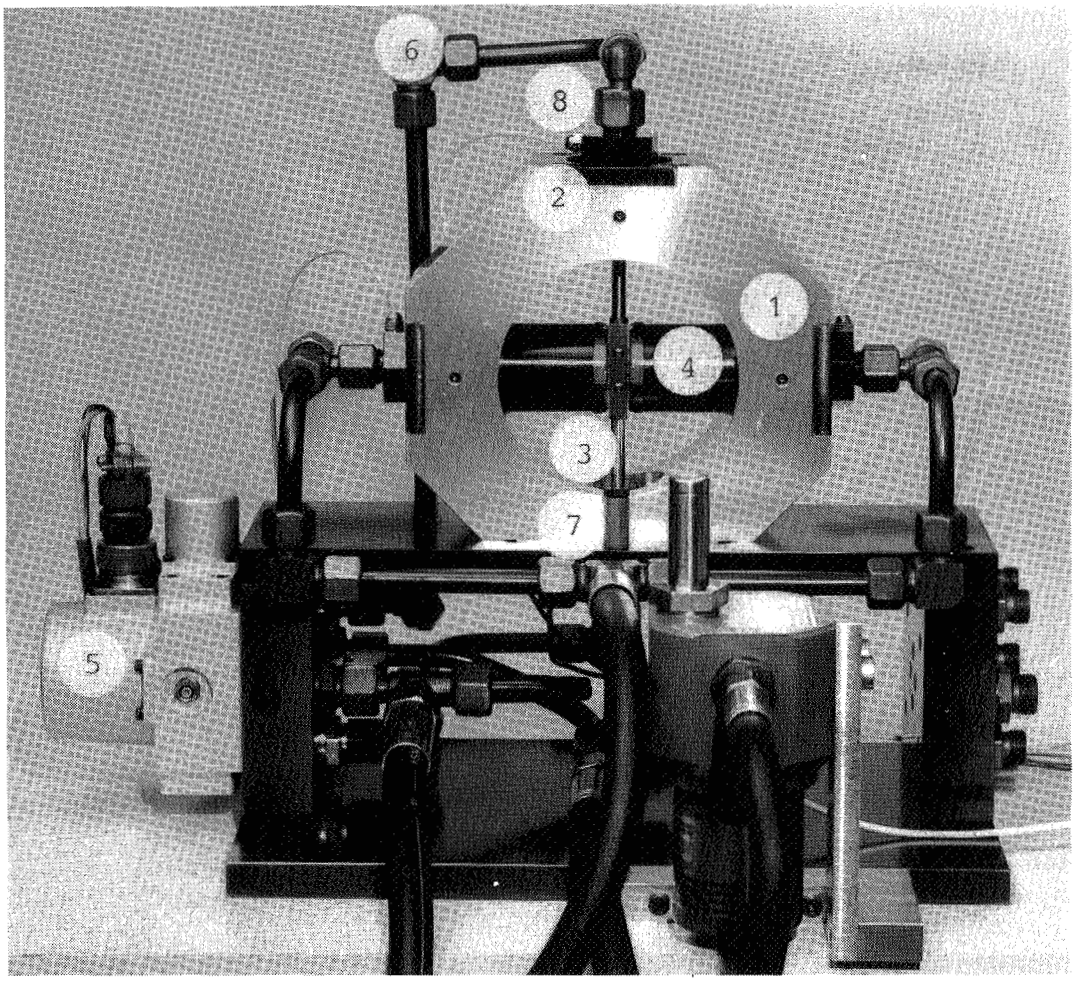

Figure 4: Test rig for active chamber system

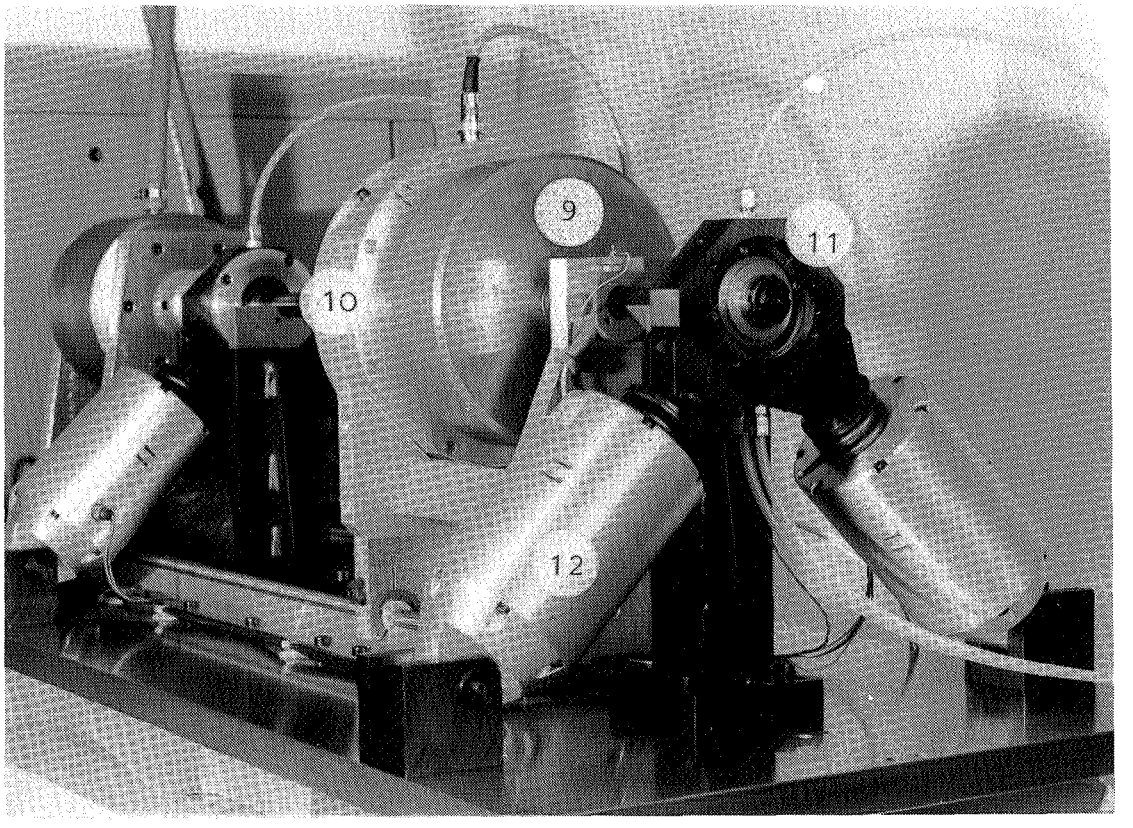

Figure 5: Test rig for rotor control

ξ_v	=	0.55		damping ratio of the servo valve
ω_v	=	1950.00	rad/s	natural frequency of the servo valve
K_{pq}	=	$4.23{\cdot}10^{-12}$	m^5/Ns	leakage coefficient
K_v	=	$1.96{\cdot}10^{-5}$	m^3/Vs	loop gain of the servo valve
A^*	=	$6.54{\cdot}10^{-4}$	m^2	characteristic membrane area
K^*	=	$4.25{\cdot}10^{-14}$	m^5/N	compressibility and membrane buckling
c_L	=	$1.63{\cdot}10^{6}$	N/m	membrane stiffness
m	=	3.41	kg	mass
U_{V0}	=	1	V	amplitude of the input voltage

Figure 6: Data for the transfer characteristic of the actuator

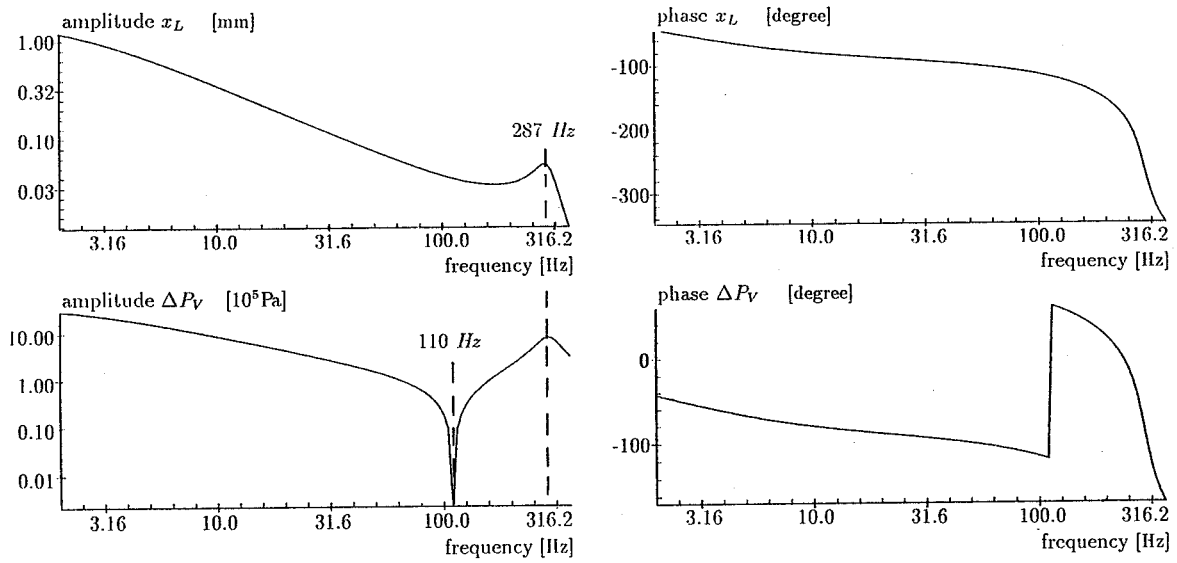

Figure 7: Simulated transfer charateristic

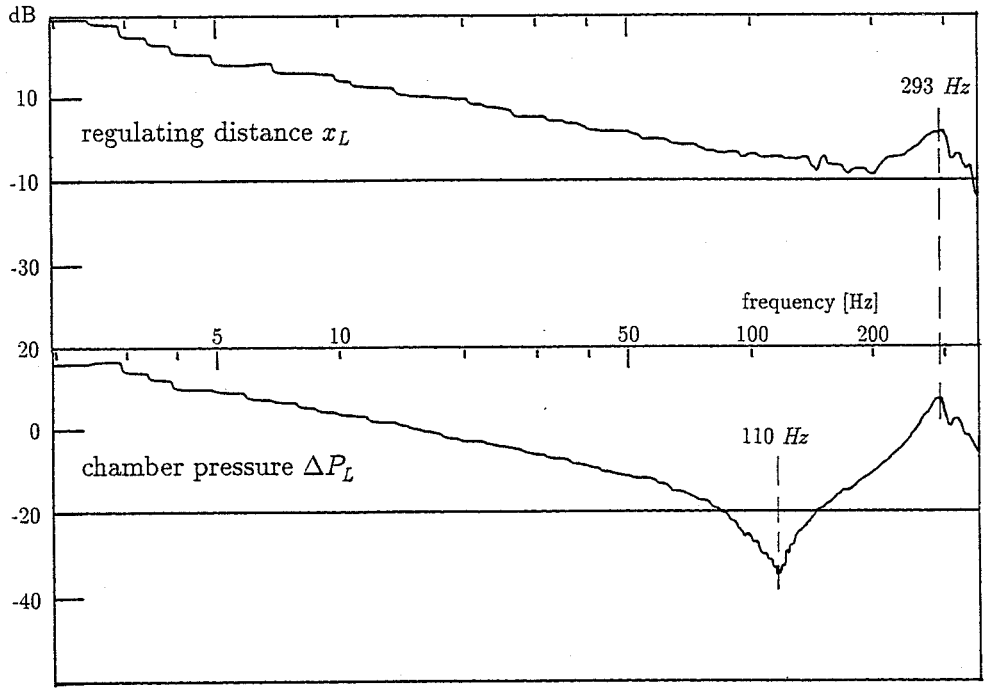

Figure 8: Measurement of the amplitude characteristic

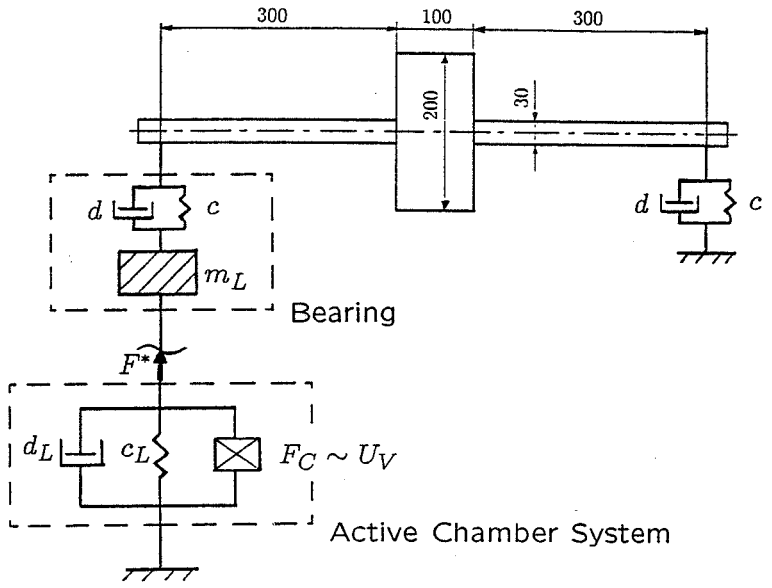

Figure 9: Geometry and mechanical model of the investigated active rotor system

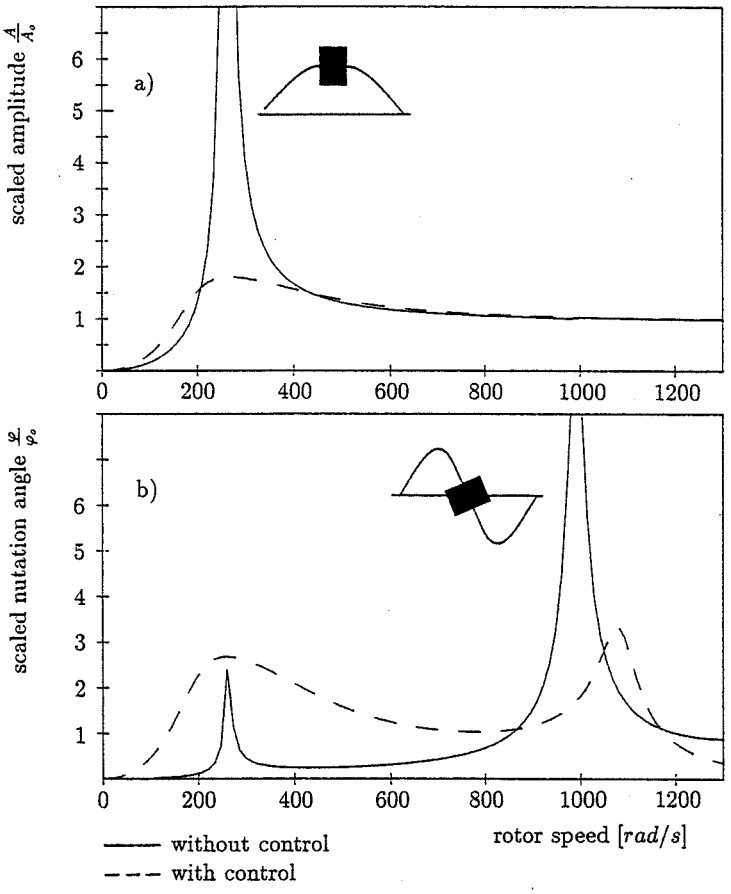

Figure 10: Response of the unbalanced rotor running through the critical speeds
a) runner displacement
b) nutation angle